Integrative Self-Assembly of Graphene Quantum Dots and Biopolymers into a Versatile Biosensing Toolkit

*Yiyang Lin, Robert Chapman, and Molly M. Stevens**

Hybrid self-assembly has become a reliable approach to synthesize soft materials with multiple levels of structural complexity and synergistic functionality. In this work, photoluminescent graphene quantum dots (GQDs, 2–5 nm) are used for the first time as molecule-like building blocks to construct self-assembled hybrid materials for label-free biosensors. Ionic self-assembly of disc-shaped GQDs and charged biopolymers is found to generate a series of hierarchical structures that exhibit aggregation-induced fluorescence quenching of the GQDs and change the protein/polypeptide secondary structure. The integration of GQDs and biopolymers via self-assembly offers a flexible toolkit for the design of label-free biosensors in which the GQDs serve as a fluorescent probe and the biopolymers provide biological function. The versatility of this approach is demonstrated in the detection of glycosaminoglycans (GAGs), pH, and proteases using three strategies: 1) competitive binding of GAGs to biopolymers, 2) pH-responsive structural changes of polypeptides, and 3) enzymatic hydrolysis of the protein backbone, respectively. It is anticipated that the integrative self-assembly of biomolecules and GQDs will open up new avenues for the design of multifunctional biomaterials with combined optoelectronic properties and biological applications.

1. Introduction

The rapid development of nanotechnology has opened up new opportunities for diagnostics and therapeutics.[1] Recently, there has been great interest in nanosized carbon dots (NanoCs), which are discrete structures less than 100 nm in size which display photoluminescence (PL) properties.[2] Unlike traditional semiconductor quantum dots (QDs), NanoCs are chemically inert, resistant to photobleaching, of low toxicity, and biocompatible. Due to their electronic and surface structure, NanoCs can give size- and wavelength-dependent multicolor emission in the visible or near-infrared (NIR) region. Upconversion luminescence from NanoCs due to anti-Stokes PL has also been observed.[3] In addition to their attractive optical properties, NanoCs can be prepared in large quantities from cheap and abundant natural carbon sources (e.g., grass, orange juice, and soy milk) through environmentally benign and readily scalable approaches. Most initial work on NanoCs focused on top-down synthetic approaches where carbon sources are cut into nanosized particles via arc discharge,[4] laser ablation,[5] electrochemical oxidation,[6] and hydrothermal.[7] Bottom-up approaches have since been developed in which NanoCs are prepared via pyrolytic decomposition, hydrothermal, and microwave pyrolysis of molecular precursors (e.g., carbohydrate, gluccerol, and amino acids).[8]

Owing to their extraordinary biocompatibility, low toxicity, tunable emission, NIR and upconversion photoluminescence, NanoCs are a promising alternative to traditional fluorescent materials (e.g., heavy metal-containing quantum dots and organic fluorophores) for in vitro or in vivo bioimaging.[9] Sun and co-workers[9a] have reported the application of a water-soluble surface passivated NanoC in cellular imaging using two-photon luminescence microscopy (excited by a 800 nm laser). At the same time, a number of bioassay methods have been developed by taking advantage of the PL of NanoCs.[10] For example, Tian and co-workers recently reported a dual-emission hybrid system by integrating NanoC and CdSe/ZnS quantum dot,[11] which they used as a ratiometric fluorescent sensor for the imaging of Cu^{2+} in HeLa cells. Photoluminescent NanoCs have also served as nanocarriers for drug delivery and gene transfection.[9b,12] Beyond the field of biology, NanoCs have shown promise in a range of applications including catalysis, organic/inorganic hybrid solar cells, carbon material-sensitized solar cells, and organic light emitting diodes (OLEDs).[13]

A promising strategy to extend the biological applications of NanoCs is to couple PL NanoCs with a diverse range of biomolecules, bringing together the advantages of both components. To this end, we hypothesized that hybrid self-assembly was an attractive route for the integration of NanoCs and biopolymers into nanomaterials in which the NanoCs not only served as PL elements but also as self-assembly building blocks. In this work, we prepared 2–5 nm graphene quantum dots (GQDs) with a disc-like shape by chemical oxidation of graphite flakes and subsequent reduction. Structurally, molecular scale sized GQDs are similar to organic dyes such as ionic porphyrin and phthalocyanine derivatives, with dominating sp^2 character and charged

Dr. Y. Lin, Dr. R. Chapman, Prof. M. M. Stevens
Department of Materials
Department of Bioengineering and Institute for Biomedical Engineering
Imperial College London
Exhibition Road, London SW7 2AZ, UK
E-mail: m.stevens@imperial.ac.uk

DOI: 10.1002/adfm.201500624

hydrophilic edges. The self-assembly of such conjugated molecules into a variety of nanostructures via multiple weak interactions (e.g., hydrophobic effect, electrostatic interactions, and hydrogen bonds) has been extensively reported to prepare organic optoelectronic materials.[14] Inspired by this, we utilized our PL GQDs as self-assembly units and coupled them with biomolecules to fabricate complex nanostructures that display biological activities. Ionic self-assembly (ISA) that takes advantage of cooperative charge interactions to provide a facile noncovalent route for the rational synthesis of soft functional materials,[14b–d,15] was used to construct hybrid GQDs/biopolymers assemblies. We show the wide applicability of this approach by assembling GQDs with a series of biopolymers (e.g., protein and polypeptide) that we used to design biosensors for glycosaminoglycans (GAGs), pH, and protease. We envision that the combination of PL carbon nanomaterials with a large group of biomolecules will lead to a class of biomaterials with novel structures and functions in diagnostic and therapeutic fields.

2. Results and Discussion

2.1. Synthesis and Characterization of GQDs

GQDs were prepared from graphite flakes using chemical oxidation in sulfuric acid/nitric acid and ultrasonic exfoliation (**Figure 1**a). Surface passivation with electron-donating or accepting groups such as primary amines is usually required to enhance PL. In contrast to these more labor-extensive routes, we found that a simple reduction of the GQDs with sodium borohydride ($NaBH_4$) resulted in an approximately fivefold enhancement in the PL (Figure S1, Supporting Information). This extraordinary increase in PL was presumed to be due to the increased number of surface defects.[16] The chemical reduction could be completed within 10 s without any conjugation chemistry and yielded water-soluble GQDs that were stable in air. The as-synthesized GQD solution was dark brown (Figure 1b) and exhibited two absorption shoulder bands at 280–310 and 340–400 nm (Figure 1c), which were

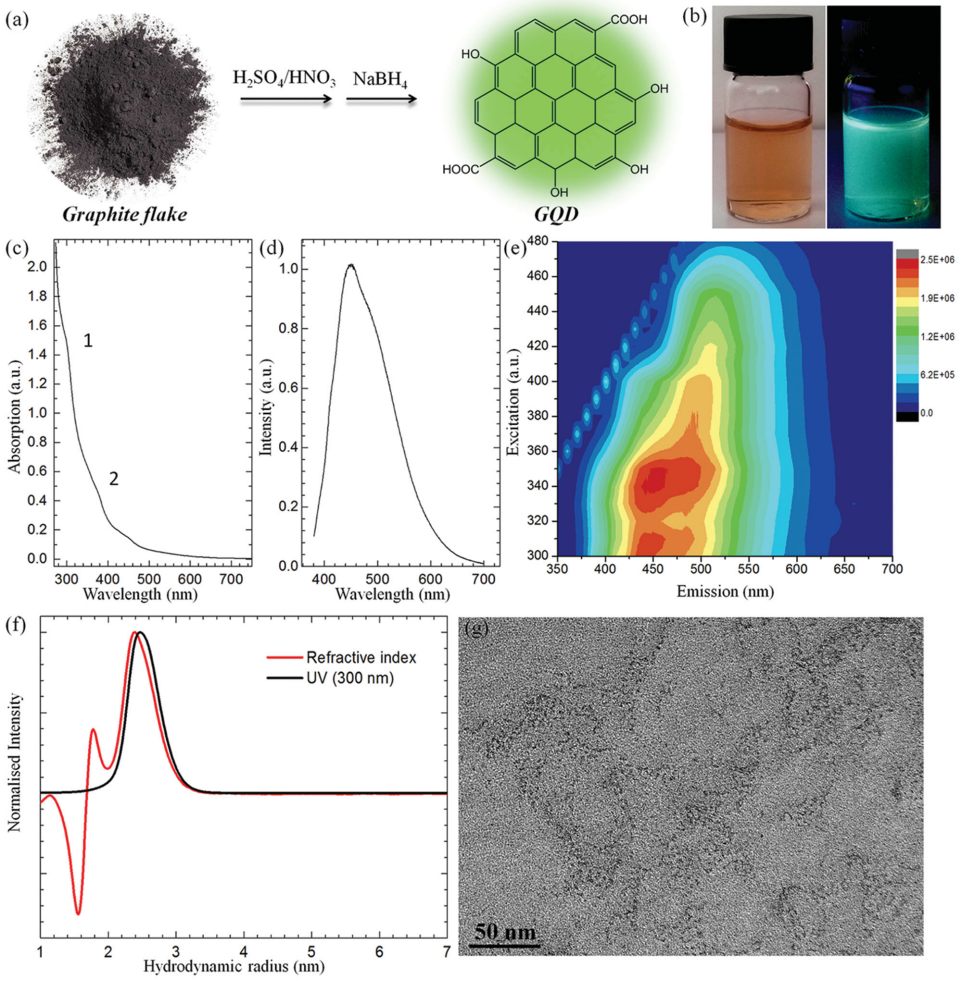

Figure 1. a) Top-down method of chemically degrading graphite into PL graphene quantum dots (GQDs) by chemical exfoliation and reduction treatment. b) Appearance of GQD solution under visible light (left) or 365 nm UV light (right). c) UV/vis and d) PL spectra of GQD solution. Two shoulder bands at 280–310 and 340–400 nm were visible in the UV/vis spectrum. e) Excitation–emission matrix (EEM) shows the phenomenon of excitation-dependent emission where a strong PL was centered at λ_{ex} = 350 nm and λ_{em} = 450 nm. f) Hydrodynamic radius of the GQDs determined by size exclusion chromatography (SEC). g) TEM image of graphene quantum dots, showing the diameter ranges between 2 and 5 nm.

ascribed to π–π^* transitions. Green photoluminescence from the GQD solution could be visualized under a 365 nm UV lamp (Figure 1b), corresponding to the emission centered at 440 nm (Figure 1d, λ_{ex} = 350 nm). The PL quantum yield of GQDs calibrated against quinine sulfate (54% in 0.1 M H_2SO_4) was found to be 1.6%. Although the origin of NanoCs photoluminescence is not yet entirely understood, there is mounting evidence the emission arises from the radiative recombination of excitons located at surface energy traps.[2a,16] As is typical for most NanoCs, excitation-dependent emission was observed as shown in the excitation–emission matrix (EEM, Figure 1e). Two emission maxima were observed at excitations of 300 and 340 nm, coinciding with the two broad shoulders in absorption spectra (Figure 1c). When the excitation wavelength was changed from 300 to 450 nm, the PL peak of GQDs was seen to shift toward higher wavelengths from 430 to 520 nm. This property is generally interpreted to be related to emissive traps or electronic conjugate structures[17] and is expected to provide the possibility for multicolor imaging.[18]

The characterization of GQDs is always difficult due to their ultrasmall size and low electron density. Here, size exclusion chromatography (SEC) was applied for the first time to investigate the size and the shape of the as-prepared GQDs. By comparing the measured retention time to a set of polyethylene oxide standards, the average hydrodynamic radius (R_h) of the GQDs was determined to be 2.4 nm (Figure 1f). The distribution of particle sizes was very narrow ($Đ$ = 1.14) and a strong absorption at 300 nm was observed, consistent with the properties of the bulk GQD solution. Some small molecular species (<2 nm) were observed using the refractive index (RI) detector, but no larger particles could be seen. Using dual angle light scattering at 15° and 90° on the SEC, we were able to estimate the form factor (R_g/R_h) of the GQDs to be 1.08, consistent with plate-shaped particles.[19] Transmission electron microscopy (TEM) was used to confirm the size and morphology of the GQDs. Since carbon atoms have lower electron density than metal atoms, it is difficult to visualize nanosized carbon materials below 10 nm. However, as shown in Figure 1g, black dots with an average diameter of 2–5 nm could be seen by TEM. Fourier-transform infrared spectroscopy (FT-IR) was performed to characterize the chemical structure of the GQDs (Figure S2, Supporting Information). The presence of carboxylic acids was confirmed by the presence of a broad peak at 3397 cm^{-1} as well as sharp peaks at 1681, 1433, and 1133 cm^{-1}, corresponding to the O—H stretching mode, the C═O stretching vibration, the C—O stretching vibration, and additional vibrations of C—OH, respectively. The peak at 1594 cm^{-1} was ascribed to C═C alkene demonstrating the sp^2 character of carbon atoms. The presence of carboxyl groups endowed excellent water solubility without any additional surface functionalization, unlike semiconductor QDs and gold nanoparticles (AuNPs) which are typically stabilized by surface ligands. Due to the dissociation of the carboxylic acids, the GQDs were found to be negatively charged at pH 7, exhibiting a ζ-potential of –15 ± 1.5 mV. While solutions of high ionic strength typically cause aggregation of traditional QD or AuNP systems, our GQDs were remarkably stable at NaCl concentrations of up to 1.5 M without obvious quenching of the PL (Figure S3, Supporting Information). In addition, the carboxyl and hydroxyl groups at the edge of the GQDs could provide a handle for conjugation of peptide, DNA, or antibody via ethyl(dimethylaminopropyl) carbodiimide/*N*-hydroxysuccinimide (EDC/NHS) coupling, a potentially easier alternative to the thiol chemistry on which surface modifications of semiconductor QDs and AuNPs typically rely.

2.2. Hybrid Self-Assembly of GQDs and Biopolymers

Due to the structural similarity of GQDs to small charged conjugated dyes that possess an extraordinary ability to self-assemble (Figure S4, Supporting Information),[14a,b,20] we anticipated that GQDs could be exploited as self-assembly building blocks. To this end, ionic self-assembly[14b,c,15a] of positively charged biopolymers and GQDs was explored with the aim of using electrostatic interactions to drive binary assembly. As expected, when the negatively charged GQDs were mixed with protamine, an arginine-rich nuclear protein, the solution's optical density (OD) gradually increased (**Figure 2**a). Since the protamine solution was transparent, this rise in OD was attributed to light scattering of newly formed particles rather than absorbance. As the protamine concentration was raised above 80 μg mL^{-1}, a sharp increase in OD was observed along with a transition in the color of solution (Figure 2a, inset). This phenomenon is analogous to surfactant self-assembly in which assembly into micelles above the critical micellar concentration (CMC) is accompanied by a sharp increase in scattered light.[21] ζ-potential measurements demonstrated that the negative GQDs were gradually neutralized by the addition of protamine, indicating the important role of electrostatic interactions in the GQD/protamine assembly (Figure 2b). At 140 μg mL^{-1} protamine, the ζ-potential plateaued at ≈+20 mV. Nanoparticle tracking analysis (NTA, Figure 2c) revealed the existence of ≈130 nm particles in the bluish GQD/protamine solution with a concentration of 2.9×10^9 particles mL^{-1}. From this, the number of protamine molecules inside each particle was estimated to be ≈10^6. TEM confirmed the presence of 100–150 nm clusters (Figure 2d–f), which exhibit a strawberry-like morphology, with small dots of 9–22 nm (12 nm on average, Figure S5, Supporting Information) decorating the surface. Since the dots are larger than a single GQD (2–5 nm), they are presumed to be formed by the aggregation of several GQDs. It is notable that the hybrid self-assembly of GQD/protamine into strawberry-like clusters could be regarded as a process of biomimetic self-assembly, which has been applied to construct hierarchical nanostructures.[22]

Interestingly, the process of GQD/protamine self-assembly into strawberry-shaped clusters was accompanied by a decrease in PL (**Figure 3**a). Although there are reports on fluorescence quenching of carbon dots by metal ions such as Cu^{2+} and Hg^{2+},[10b,11,23] it is unusual that a protein or biomolecule should quench GQDs since the quenching of carbon dots by metal ions is normally regulated by a nonradiative recombination of excitons through an effective electron transfer.[24] Given that protamine itself cannot quench the GQDs, it is believed the PL quenching in GQD/protamine is due to the aggregation of GQDs (Figure 2d–f) facilitating nonradiative energy transfer. Since the PL of GQDs depends on their aggregation state, they could be used as a self-indicative probe, like fluorescence

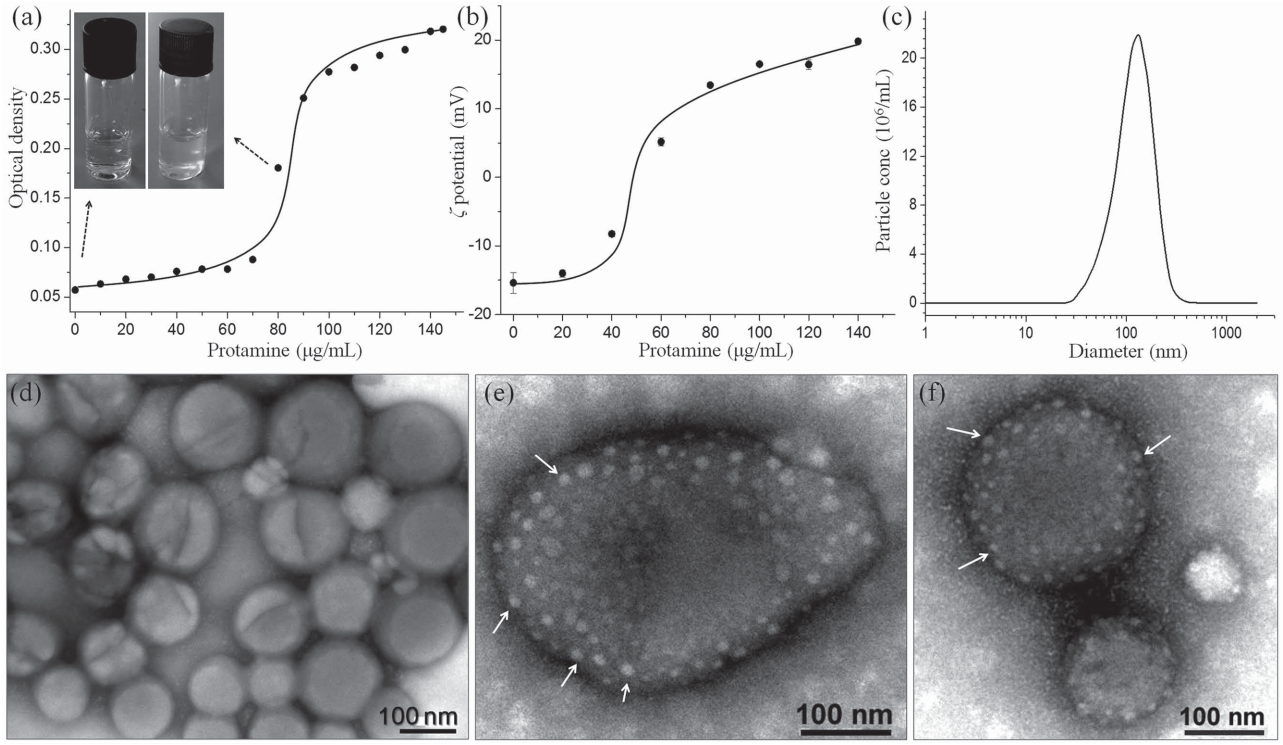

Figure 2. a) Optical density and b) ζ-potential of GQDs solution upon the addition of protamine. The insets in (a) show macroscopic pictures of the GQD/protamine solution (right) which is bluish, and GQDs solution (left) which is clear. c) Nanosight tracking analysis of GQD/protamine solution shows the size and concentration of hybrid clusters. e,f) TEM images of GQD/protamine show spherical strawberry-like clusters with the diameter of 100–200 nm. The arrows in (e) and (f) indicate the small dots are formed by aggregated GQDs. The TEM samples are prepared by a negative staining technique using 1% uranyl acetate.

probes, to monitor the self-assembly process. Maximum PL quenching was observed at 80 μg mL^{-1} protamine (Figure 3a), which was the same concentration at which the strawberry-shaped clusters were observed to form by OD measurements (Figure 2a). In addition, PL was found to be a more sensitive way to track the self-assembly process than OD as noticeable PL changes were observed at small amounts of protamine (Figures 2a and 3a). This is likely because the fluctuation OD depends on the size changes of cluster formation while PL is related to the aggregation of GQD that happens even when clusters are very small.

Aggregation-induced quenching of GQD PL was also observed with other positive biopolymers including poly-L-histidine (PLH), polyethylenimine (PEI), poly-L-arginine (PLR), and poly-L-lysine (PLL) (Figure 3b). The formation of hierarchical structures in GQD/PLL, GQD/PLH, GQD/PLR, and GQD/PEI was confirmed by TEM. As shown in Figure 3c–e, interconnected networks were observed in GQD/PLL, GQD/PLR, and GQD/PLH mixtures possibly owing to the bridging effect of polymer chains. However, micrometer-sized coacervate larger than 1 μm were formed in the GQD/PEI solution, structurally similar to the peptide/nucleotide microdroplet reported by Mann[25] as a membrane-free protocell model. We speculate the spherical shape of these aggregates is largely due to the branched molecular structures of PEI compared to the linear polypeptides (i.e., PLH, PLL, and PLR). No quenching of the GQDs was observed when they were mixed with anionic or nonionic polymers such as bovine serum albumin (BSA), human serum albumin (HSA), heparin, or polyethylene glycol (PEG, 5K) (Figure 3b). This confirmed the essential role of electrostatic interactions in hybrid self-assembly of GQD/biopolymer. Because the surface properties of GQDs can be tailored by surface passivation with PEI or 4,7,10-trioxa-1,13-tridecanediamine,[9b,26] we hypothesized a similar method could be used to prepare positively charged NanoCs, which could be used to complex with anionic biomolecules.

The hybrid self-assembly of biopolymers and GQDs was found to be associated with the onset of polypeptide or protein secondary structure. As shown in **Figure 4**a, the circular dichroism (CD) spectra of poly-L-lysine solution showed a negative band at 196 nm corresponding to the π–π^* transition and a positive band at 217 nm corresponding to the n–π^* transition, indicating a random coil structure. Upon addition of GQDs, the intensity of the 192 nm band decreased and that of the two bands at 210 and 225 nm increased. These two peaks corresponded to the π–π^* and n–π^* transitions, respectively, in the α-helical peptide secondary structure, suggesting that the hybrid self-assembly of poly-L-lysine/GQDs induced a random coil-to-helix transition in the peptide. We suspect the stabilization of the α-helical structure in the hybrid system is due to the charge screening of the lysine side chains by the GQDs in combination with local stacking of planar GQDs anions around the helix secondary structure. This peptide helix-assisted GQD aggregation eventually leads to the aggregation-induced quenching of the GQD

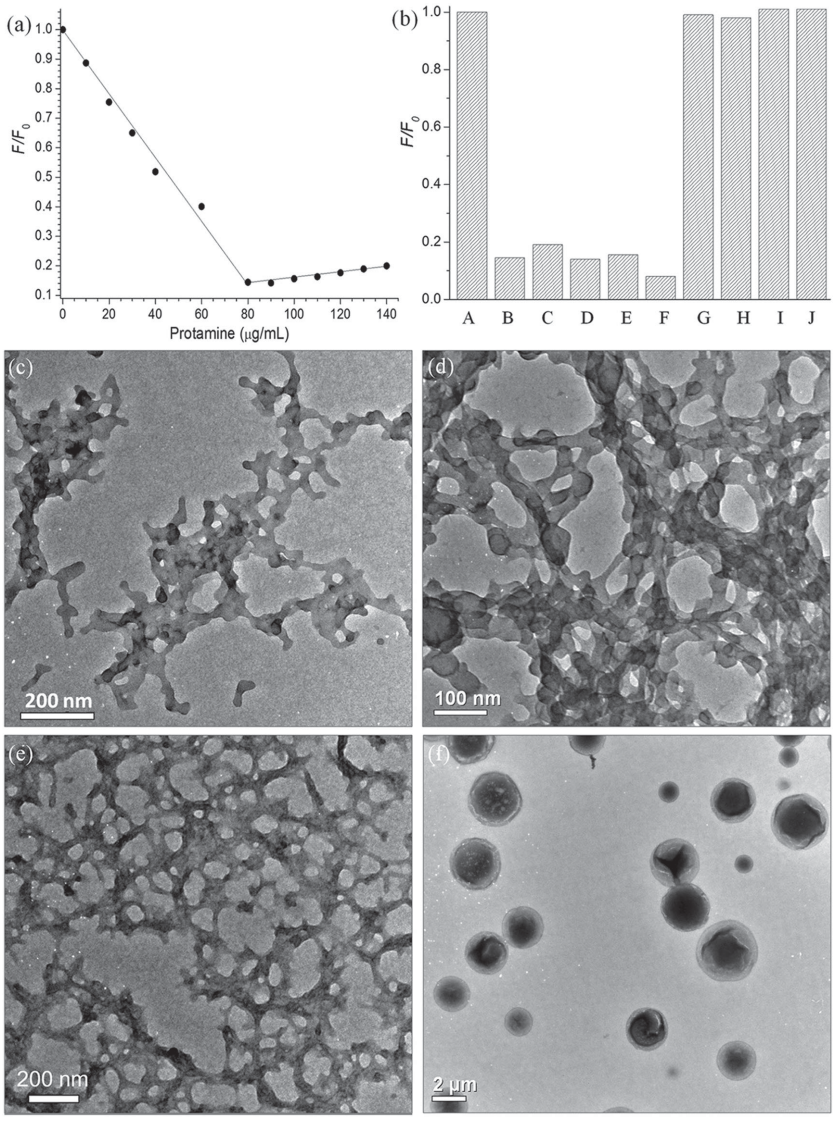

Figure 3. a) Variation of PL intensity in GQD solution upon the addition of protamine, showing the PL quenching of GQDs up to 85% (λ_{ex} = 350 nm, λ_{em} = 450 nm). b) Effects of different biopolymers on PL intensity of GQDs where cationic polymers exhibit significant quenching effect while anionic or nonionic polymers have no similar effect. A) Control, B) PLH, C) PLL, D) protamine, E) PLR, F) PEI, G) BSA, H) HSA, I) PEG, J) heparin. TEM images of hybrid self-assembled nanostructures from c) GQD/PLH, d) GQD/PLR, e) GQD/PLL, and f) GQD/PEI.

PL (Figure 3a). Similar polypeptide conformation changes were observed in poly-L-arginine/GQDs mixtures (Figure 4b) but not in protamine/GQDs and poly-L-histidine/GQDs (Figure 4c,d). Although the random coil-to-helix transition has been reported in polypeptide solutions by varying the solution pH or ionic strength,[27] to our knowledge the use of nanomaterials to give rise to secondary structural changes is rare.

2.3. Multifunctional Biosensing Based on GQD/Biopolymer Self-Assembly

An important feature of noncovalent self-assembly is the dynamic and adaptive nature that allows controllable aggregation/disaggregation of hybrid GQD/biopolymer systems by chemical or biological stimuli (e.g., pH and enzyme). Such a process should be accompanied by the change in GQD PL, enabling the design of label-free biological sensors. This concept was used to build multifunctional biosensing platforms for GAG, pH, and protease based on three mechanisms: competitive binding of GAGs to protein, pH-responsive structural change of polypeptides, and enzymatic digestion of protein, respectively.

GAGs are a subfamily of carbohydrate polymers that display various biological functions such as regulation of cell growth. Subtle changes in the GAG structures (e.g., charge, acetylation, and sulfonation) can significantly affect their biological activity. Despite the effort devoted to the detection of heparin, the identification of GAGs is difficult due to their similar disaccharide repeated units.[28] Here, GAG sensing and discrimination was achieved via competitive GAG/protein complexation in a GQD/protein self-assembled system, leading to the dissociation of GQD/protein aggregates and recovery of GQD PL. Initially, we used the GQD/protamine clusters to detect heparin, a natural sulfated polysaccharide used as an anticoagulant/antithrombotic agent during clinical procedures. Heparin is a highly negatively charged GAG (≈70 negative charges)[29] and is known to form strong complexes with the highly positively charged, arginine-rich protamine ($\bar{M}_w$ = 4500 Da, pI = 13.8).[29] We hypothesized that the strength of this interaction should result in dissociation of the GQD/protamine clusters upon addition of heparin and release of the GQDs. As expected, heparin was found to restore the photoluminescence of GQDs, presumably due to its preferential binding with protamine (**Figure 5**a), even at very low concentrations (1.0 μg mL^{-1}) below those used in the aforementioned clinical procedures (1.2–48 μg mL^{-1}).[30] The presence of other substances such as Ca^{2+}, Mg^{2+}, and glutathione at biologically relevant concentrations does not significantly interfere with the assay as shown in Figure S7, Supporting Information.

The use of GAG/protamine complexation to disrupt the GQD/protamine self-assembly was further exploited to discriminate six GAGs including heparin (G1), *N*-acetyl-de-*O*-sulfated heparin sodium (G2), hyaluronic acid sodium (G3), dextran sulfate (G4), chondroitin sulfate (G5), and chitosan (G6) (Figure 5b). In principle, a stronger GAG/protamine complex should allow for a better displacement of quenched GQDs by GAGs and result in a higher PL enhancement in the GQD/protamine system. As shown in **Figure 6**c, the addition of the various GAGs increased the PL with varying efficacy in the order: G4 > G1 > G5 > G2, G3 > G6. These efficacy differences could

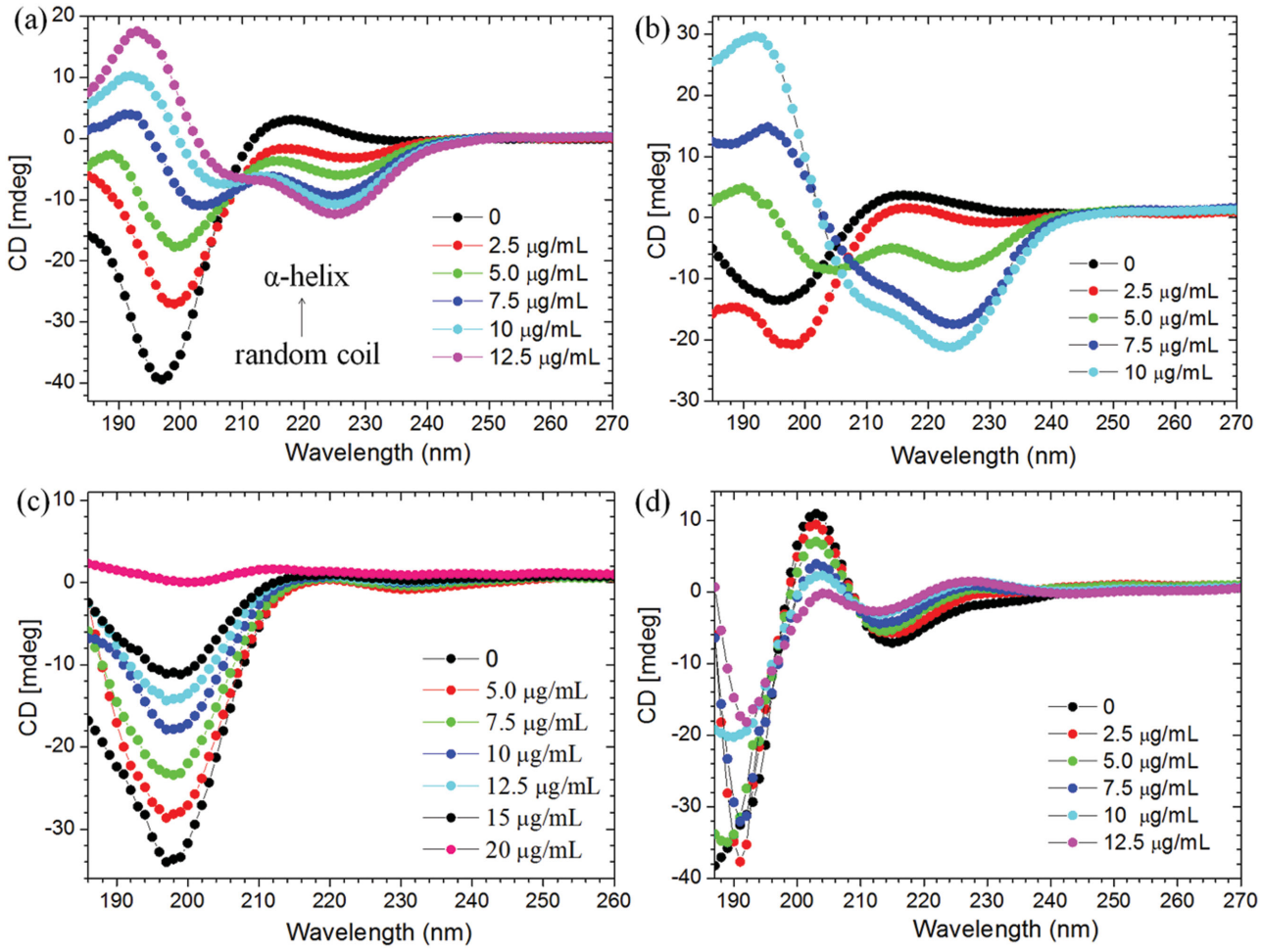

Figure 4. Circular dichroism (CD) spectra of biopolymers in the presence of GQDs: a) poly-L-lysine; b) poly-L-arginine; c) protamine; d) poly-L-histidine. The concentration of biopolymers was 200 μg mL^{-1}. The conformational transition of polypeptide from random coil to α-helix was observed in (a,b). The coil structures in (c,d) were weakened. Poly-L-lysine and poly-L-histidine were dispersed in pH 5.5 and pH 7.5, respectively.

be rationalized by analyzing the molecular structure of the GAGs. All GAGs consist of disaccharide repeating units with different hydrophilic groups on the backbones (Figure 5b). Because of their negative charge, it is likely that the anionic carboxyl, sulfonate, and sulfate groups are responsible for the formation of GAG/protamine complex. As summarized in Figure 5d, G4 and G1 possess four negative charges on each repeating unit, and therefore recover the PL most efficiently. G5 and G2 contain two negative charges on each disaccharide unit and show a lower PL recovery effect, while G3 contains only one carboxyl group and has an even lower efficiency. The greater recovery of PL by G4 than G1 could not be explained by direct comparison of total charge, but can be explained by the concept of charge distribution. According to the quantum-chemical calculation (AM1 method),[31] the effective charge on different ionic groups is not the same but is weaker for carboxylic acid (–0.894) and sulfonate groups (–0.465) than for sulfate groups (–1.071). Since G4 contains four of the more "negative" sulfate groups, its overall charge would be expected to be more negative than G1 which contains only three, and so would be expected to give rise to greater PL recovery. Similarly, it is not surprising that G5 restores the PL more efficiently than G2 because G5 is more "negative." In this way, GAG discrimination was achieved by measuring the PL enhancement in GQD/protamine mixtures, which is also indicative of the intensity of GAG/protamine interactions. In addition, by using statistical techniques such as linear discriminant analysis (LDA), the hybrid self-assembly of GQDs and biopolymers could be used as a sensor array for quantitative detection of GAGs.[32]

Sensors that monitor pH have attracted a great deal of recent attention since intracellular pH plays a pivotal role in cell metabolism processes such as the proliferation and apoptosis.[33] In this study, we used the integrative self-assembly of GQD/biopolymer to construct a pH sensing platform. PLH was used because of the imidazole moieties it contains, the pK_a of which (≈6.0) is within the physiologically relevant pH range.[34] Similar to the GQD/protamine system, the hybrid self-assembly of GQD/PLH was confirmed by the aggregation-induced quenching of GQD PL (Figure 6a). As shown in Figure 6a, the addition of PLH at pH 5.5 resulted in a gradual decrease of GQD PL, with maximum quenching (≈80 %) achieved after addition of 40 μg mL^{-1} of PLH. At this pH, the imidazole

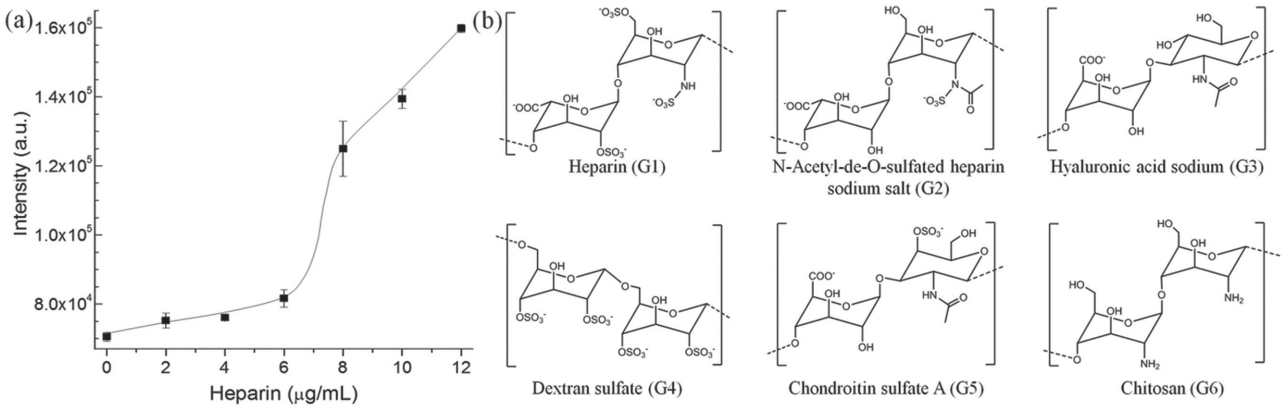

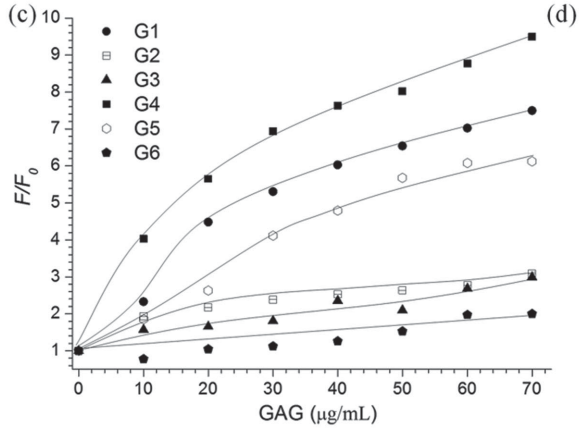

(d)

	-COONa	-SO_3Na	-SO_4Na	-OH
Heparin (G1)	1	1	2	2
N-Acetyl-de-O-sulfated heparin sodium salt (G2)	1	1	0	4
Hyaluronic acid sodium (G3)	1	0	0	4
Dextran sulfate (G4)	0	0	4	2
Chondroitin sulfate A (G5)	1	0	1	3
Chitosan (G6)	0	0	0	4

Figure 5. a) PL intensity of GQD/protamine solutions (λ_{ex} = 350 nm and λ_{em} = 450 nm) upon the addition of heparin. The concentration of protamine is 80 μg mL^{-1} and GQD is 50 μg mL^{-1}. b) Molecular structures of glycosaminoglycans (GAGs) used in this work: heparin (G1), *N*-acetyl-de-*O*-sulfated heparin sodium (G2), hyaluronic acid sodium (G3), dextran sulfate (G4), chondroitin sulfate A (G5), and chitosan (G6). c) PL response of GQD/protamine solutions (λ_{ex} = 350 nm and λ_{em} = 450 nm) in the presence of GAGs. d) Analysis and comparison of GAGs structures regarding to the hydrophilic groups. Acetate buffer (10×10^{-3} M, pH 5.5) was used in GQD/polyhistidine to ensure the complete ionization of histidine groups while phosphate buffer (10×10^{-3} M, pH 7.5) was used in all the other experiments.

groups of the PLH will be ionized and positively charged, and the resulting electrostatic self-assembly of GQD/PLH drives the loss of PL. The quenched fluorescence of the GQDs could be recovered by raising the solution pH. A PL enhancement in excess of fivefold was obtained as the pH was increased from 7.0 to 9.5, and most of the original fluorescence was recovered (Figure 6b). Since the photoluminescence of GQDs remained unchanged across the pH range from 5.5 to 9.5 (Figure S6, Supporting Information), the PL enhancement in GQD/PLH cannot be from any change in the GQDs themselves. Rather, as the pH is increased, the deionization of imidazole groups on PLH would be expected to weaken the electrostatic attractions, and the resulting dissociation of the GQD/PLH clusters explains the restoration of the PL of GQDs observed experimentally. As expected, a critical point was observed at pH 6.7, at which 80% of the imidazole groups should be deionized (Figure 6c). In addition, the dynamic pH range can be shifted to 5–8.5 by varying the GQD/PLH ratio (Figure S8, Supporting Information). It is well-known that pH in tumor and inflammatory tissues is lower than in normal tissue, with endosomes and lysosomes exhibiting even lower pH values. We anticipate this sensing platform could be further optimized as an in vivo tumor sensor due to its low cytotoxicity and biocompatibility. Given the wide variety of proteins or peptides that have different protonation/deprotonation properties, our platform is expected to provide pH sensing across broad pH ranges. For example, by using PLL (which has a pK_a of ≈9),[35] instead of PLH to drive the assembly of the clusters, the recovery of the GQD PL was observed instead at pH > 9 (Figure 6b).

Finally, the GQD/protamine clusters were used to develop a label-free trypsin sensor. As the most important digestive enzyme, trypsin is secreted by the pancreas and involved in the digestive enzyme activation cascade.[36] The trypsin level is also closely related with some types of pancreatic diseases.[37] Because it is rich in arginine, protamine can be readily hydrolyzed by trypsin and used as trypsin substrate.[38] We incubated our self-assembled GQD/protamine mixture with trypsin and recorded the photoluminescence after 3 h. As shown in **Figure 7**a, a marked PL recovery was observed after this incubation. The limit of detection (LOD), defined as the lowest assayed concentration of enzyme which yielded a signal higher than three times the standard deviation of blank, was determined to be 0.1×10^{-9} M. This value is three orders lower than that of commercial kits (≈0.5 μg mL^{-1} or 21×10^{-9} M) which use fluorescein isothiocyanate (FITC) labelled casein as a substrate. The enhancement of GQDs PL was found to be accompanied by the

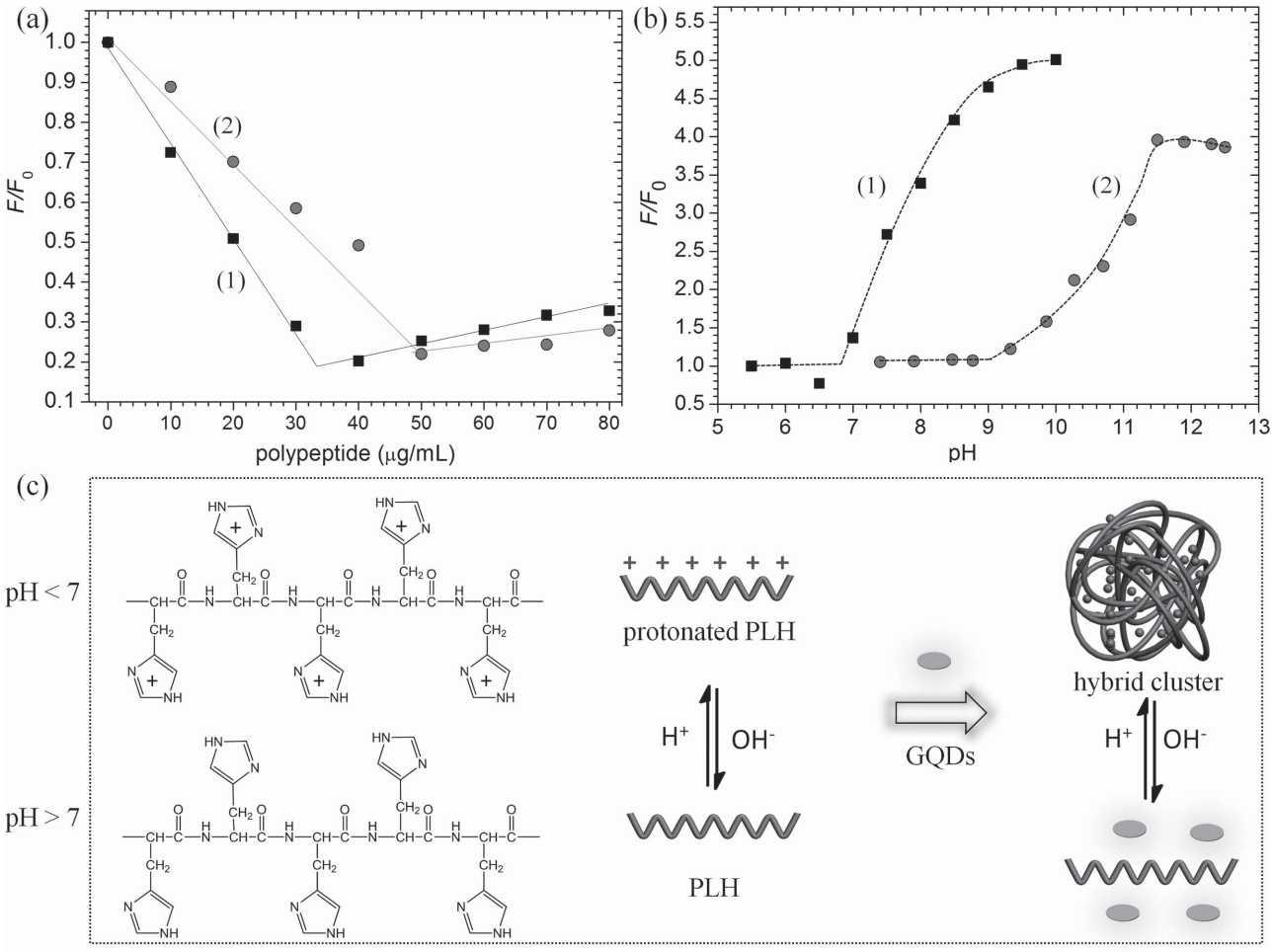

Figure 6. a) Photoluminescence of GQDs solution (λ_{ex} = 350 nm and λ_{em} = 450 nm) in the presence of different amounts of PLH at pH 5.5 (1) and PLL at pH 7.5 (2). b) PL variations of GQD/PLH (1) and GQD/PLL (2) solutions at different pHs, where emission enhancement is noted from pH 7.0 to 9.5 (gray area) for GQD/PLH, and from pH 9.2 to 11.5 (pink area) for GQD/PLL. c) Structural changes of PLH molecule via protonation or deprotonation of imidazole groups at different pHs. pH-dependence of GQD/PLH interaction and their self-assembly behaviors are depicted.

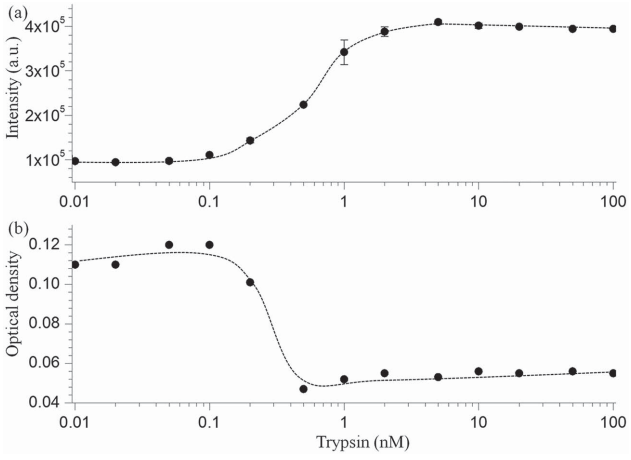

Figure 7. a) Photoluminescence (PL) and b) optical density (OD) of the solution of GQD/protamine clusters in the presence of different concentrations of trypsin.

decrease of solution OD (Figure 7b), implying the disassembly of GQD/protamine aggregate after trypsin digestion. Given the extensive library of protease-cleavable protein and peptides,[39] the integrative self-assembly of GQD/biopolymer is expected to enable the sensitive detection of a variety of enzymes.

3. Conclusion

Photoluminescent GQDs were synthesized from graphite powders combined with top-down oxidation and subsequent chemical reduction. The obtained disk-shaped GQDs (2–5 nm) exhibit extraordinary stability in aqueous solutions against high concentrations of salt and long-term storage. To our knowledge, GQDs were exploited for the first time as building blocks to create hybrid nanostructures via ionic self-assembly of GQDs and biopolymers, which lead to aggregation-induced quenching of GQD PL and secondary structural changes of polypeptides and proteins. Label-free platforms were developed for the simple and reliable bioanalysis of pH, glycosaminoglycans,

and protease based on the integrative self-assembly of GQD/biopolymer. By utilizing the competitive binding of various GAGs to protamine, we have demonstrated the sensitive detection of heparin as well as the discrimination of six different GAGs from the PL recovery of GQD/protamine solutions. Our results emphasize the importance of charge distribution on the hydrophilic headgroups of GAGs on GAG/protein interactions. By incorporating pH- and enzyme-sensitive biopolymers into the binary self-assembly, we designed a trypsin sensor and a class of pH sensors with adjustable pH-sensitive zones. We anticipate the integration of GQDs and a variety of biomolecules via noncovalent self-assembly will provide a series of functional biomaterials that simultaneously possess bioactivities and optical properties. The hybrid self-assembly of GQD/biopolymer is a promising approach by which to generate nanocarriers for drug, protein, and DNA, and which will offer the therapeutic action and image the results for the treatment of disease.

4. Experimental Section

Materials: Graphite powder, trypsin from bovine pancreas, poly-L-lysine hydrobromide (wt 4000–15 000), poly-L-arginine hydrochloride (wt 15 000–70 000), poly-L-histidine (wt 5000–25 000), protamine sulfate from salmon, heparin, dextran sulfate sodium salt from *Leuconostoc* spp. (wt > 500 000), *N*-acetyl-de-*O*-sulfated heparin sodium, hyaluronic acid sodium salt from *Streptococcus equi*, dextran sulfate, chondroitin sulfate A, chitosan (medium molecular weight), trypsin from bovine pancreas (TPCK-treated, essentially salt-free, lyophilized powder, ≧10 000 BAEE units mg^{-1} protein), and the other chemicals were obtained from Sigma-Aldrich and used without further purification. Spectra/Por 6 dialysis tubing, 1000 MWCO was obtained from Spectrum Europe BV. Water was purified using a Millipore filtration system.

Synthesis of Graphene Quantum Dots (GQDs): The synthetic method of GQDs was similar to literature[40] except sodium borohydride was introduced to increase the photoluminescence quantum yield. In detail, graphite flakes (100 mg) were mixed with sulfuric acid (15 mL) and nitric acid (5 mL) in a 50 mL flask and refluxed for 24 h at 80 °C. The reaction mixture was diluted with 100 mL water and dialyzed in a dialysis bag (MWCO 1000) against deionized water to remove excess acid. The product was filtered with a 0.1 μm microfilm filter to remove large particles. Reduction treatment was conducted by introducing 1 x 10^{-3} M $NaBH_4$ and purified by dialysis through a dialysis bag (MWCO 1000). The product was stored in dark for further use.

Size Exclusion Chromatography (SEC): SEC was performed on an Agilent 1260 GPC equipped with RI, light scattering (15° and 90°), UV and viscometry detectors in 0.5 × PBS as the eluent. Separation was performed over two PL gel mixed-M columns in series at 25 °C. The hydrodynamic volume was measured relative to a set of polyethylene oxide (PEO) standards of known M_Ws using the RI detector. The hydrodynamic radius of the PEO standards was calculated according to the equation below[41]

$$R_h = 0.145 \times M_W^{0.571 \pm 0.009} \quad (1)$$

Characterization: TEM images were obtained with a JEOL 2000FX and 2010 (working voltage of 200 kV) by negative-staining method with uranyl acetate solution (1.0 wt%) as the staining agent. Fluorescence measurements were recorded on Fluorolog-3 spectrofluorometer. ζ-potential were measured on a Malvern Zetasizer Nano ZS (Malvern, UK) with a backscattering detection at 173° equipped with a He–Ne laser (λ = 632.8 nm). Nanoparticle tracking and analysis measurements were performed with a NanoSight LM20. Videos of 60 s length were recorded for analysis, and the measurements were repeated to verify results.

Quantum Yield Calculation: Photoluminescence quantum yield of graphene quantum dots was obtained using the comparative method with quinine sulfate (54% in 0.1 M H_2SO_4) as a standard fluorophore.

Trypsin Assay: Trypsin stock solutions were prepared in 1.0 × 10^{-3} M hydrogen chloride solution and stored at −20 °C. The trypsin activity test was conducted in 5 × 10^{-3} M phosphate buffer (pH 8.5) and the photoluminescence of GQDs was measured on Fluorolog-3 spectrofluorometer (λ_{ex} = 350 nm, λ_{em} = 450 nm).

Circular Dichroism (CD): CD experiments were conducted on a Dichroism Spectropolarimeter Jasco 715. The temperature was maintained at 20 °C by a water bath. CD spectra were the average of three scans obtained by collecting data from 270 to 185 nm. poly-L-histidine and poly-L-lysine were dissolved in the buffer solution of pH 5.5 and 7.5, respectively.

Supporting Information

Supporting Information is available from the Wiley Online Library or from the author.

Acknowledgements

M.M.S. thanks the EPSRC grants (EP/K020641/1 and EP/K502352/1) and ERC Consolidator grant Naturale-CG for funding.

Received: February 13, 2015
Revised: March 14, 2015
Published online: April 15, 2015

[1] a) P. D. Howes, S. Rana, M. M. Stevens, *Chem. Soc. Rev.* **2014**, *43*, 3835; b) P. D. Howes, R. Chandrawati, M. M. Stevens, *Science* **2014**, *346*, 1247390.

[2] a) S. N. Baker, G. A. Baker, *Angew. Chem. Int. Ed.* **2010**, *49*, 6726; b) J. Shen, Y. Zhu, X. Yang, C. Li, *Chem. Commun.* **2012**, *48*, 3686; c) Z. Zhang, J. Zhang, N. Chen, L. Qu, *Energy Environ. Sci.* **2012**, *5*, 8869.

[3] J. Shen, Y. Zhu, C. Chen, X. Yang, C. Li, *Chem. Commun.* **2011**, *47*, 2580.

[4] X. Y. Xu, R. Ray, Y. L. Gu, H. J. Ploehn, L. Gearheart, K. Raker, W. A. Scrivens, *J. Am. Chem. Soc.* **2004**, *126*, 12736.

[5] Y. P. Sun, B. Zhou, Y. Lin, W. Wang, K. A. S. Fernando, P. Pathak, M. J. Meziani, B. A. Harruff, X. Wang, H. F. Wang, P. J. G. Luo, H. Yang, M. E. Kose, B. L. Chen, L. M. Veca, S. Y. Xie, *J. Am. Chem. Soc.* **2006**, *128*, 7756.

[6] a) H. Li, X. He, Z. Kang, H. Huang, Y. Liu, J. Liu, S. Lian, C. H. A. Tsang, X. Yang, S.-T. Lee, *Angew. Chem. Int. Ed.* **2010**, *49*, 4430; b) L. Bao, Z.-L. Zhang, Z.-Q. Tian, L. Zhang, C. Liu, Y. Lin, B. Qi, D.-W. Pang, *Adv. Mater.* **2011**, *23*, 5801; c) H. Liu, T. Ye, C. Mao, *Angew. Chem. Int. Ed.* **2007**, *46*, 6473.

[7] a) S. Liu, J. Tian, L. Wang, Y. Zhang, X. Qin, Y. Luo, A. M. Asiri, A. O. Al-Youbi, X. Sun, *Adv. Mater.* **2012**, *24*, 2037; b) S. Sahu, B. Behera, T. K. Maiti, S. Mohapatra, *Chem. Commun.* **2012**, *48*, 8835; c) L. Tang, R. Ji, X. Cao, J. Lin, H. Jiang, X. Li, K. S. Teng, C. M. Luk, S. Zeng, J. Hao, S. P. Lau, *ACS Nano* **2012**, *6*, 5102; d) S. Zhu, Q. Meng, L. Wang, J. Zhang, Y. Song, H. Jin, K. Zhang, H. Sun, H. Wang, B. Yang, *Angew. Chem. Int. Ed.* **2013**, *52*, 3953.

[8] a) H. Zhu, X. Wang, Y. Li, Z. Wang, F. Yang, X. Yang, *Chem. Commun.* **2009**, 5118; b) X. Wang, K. Qu, B. Xu, J. Ren, X. Qu, *J. Mater. Chem.* **2011**, *21*, 2445.

[9] a) L. Cao, X. Wang, M. J. Meziani, F. Lu, H. Wang, P. G. Luo, Y. Lin, B. A. Harruff, L. M. Veca, D. Murray, S.-Y. Xie, Y.-P. Sun, *J. Am. Chem. Soc.* **2007**, *129*, 11318; b) J. Kim, J. Park, H. Kim, K. Singha,

W. J. Kim, *Biomaterials* **2013**, *34*, 7168; c) X. L. Huang, F. Zhang, L. Zhu, K. Y. Choi, N. Guo, J. X. Guo, K. Tackett, P. Anilkumar, G. Liu, Q. M. Quan, H. S. Choi, G. Niu, Y. P. Sun, S. Lee, X. Y. Chen, *ACS Nano* **2013**, *7*, 5684.

[10] a) W. Shi, X. Li, H. Ma, *Angew. Chem. Int. Ed.* **2012**, *51*, 6432; b) I. Costas-Mora, V. Romero, I. Lavilla, C. Bendicho, *Anal. Chem.* **2014**, *86*, 4536.

[11] A. Zhu, Q. Qu, X. Shao, B. Kong, Y. Tian, *Angew. Chem. Int. Ed.* **2012**, *51*, 7185.

[12] X. Sun, Z. Liu, K. Welsher, J. T. Robinson, A. Goodwin, S. Zaric, H. Dai, *Nano Res.* **2008**, *1*, 203.

[13] a) Z. Xie, F. Wang, C.-Y. Liu, *Adv. Mater.* **2012**, *24*, 1716; b) V. Gupta, N. Chaudhary, R. Srivastava, G. D. Sharma, R. Bhardwaj, S. Chand, *J. Am. Chem. Soc.* **2011**, *133*, 9960; c) Y. Li, Y. Hu, Y. Zhao, G. Shi, L. Deng, Y. Hou, L. Qu, *Adv. Mater.* **2011**, *23*, 776; d) X. Yan, X. Cui, B. Li, L.-S. Li, *Nano Lett.* **2010**, *10*, 1869.

[14] a) A. D. Schwab, D. E. Smith, B. Bond-Watts, D. E. Johnston, J. Hone, A. T. Johnson, J. C. de Paula, W. F. Smith, *Nano Lett.* **2004**, *4*, 1261; b) K. E. Martin, Z. Wang, T. Busani, R. M. Garcia, Z. Chen, Y. Jiang, Y. Song, J. L. Jacobsen, T. T. Vu, N. E. Schore, B. S. Swartzentruber, C. J. Medforth, J. A. Shelnutt, *J. Am. Chem. Soc.* **2010**, *132*, 8194; c) D. Franke, M. Vos, M. Antonietti, N. Sommerdijk, C. F. J. Faul, *Chem. Mater.* **2006**, *18*, 1839; d) Q. Zhao, Y. Wang, Y. Qiao, X. Wang, X. Guo, Y. Yan, J. Huang, *Chem. Commun.* **2014**, *50*, 13537.

[15] a) C. F. J. Faul, M. Antonietti, *Adv. Mater.* **2003**, *15*, 673; b) M. Antonietti, J. Conrad, *Angew. Chem. Int. Ed.* **1994**, *33*, 1869; c) T. Kato, N. Mizoshita, K. Kishimoto, *Angew. Chem. Int. Ed.* **2006**, *45*, 38; d) K. Watanabe, H. Iida, K. Akagi, *Adv. Mater.* **2012**, *24*, 6451; e) C. F. J. Faul, *Acc. Chem. Res.* **2014**, *47*, 3428.

[16] R. Shen, K. Song, H. Liu, Y. Li, H. Liu, *Chem. Phys. Chem.* **2012**, *13*, 3549.

[17] M. Zhang, L. Bai, W. Shang, W. Xie, H. Ma, Y. Fu, D. Fang, H. Sun, L. Fan, M. Han, C. Liu, S. Yang, *J. Mater. Chem.* **2012**, *22*, 7461.

[18] R. Liu, D. Wu, S. Liu, K. Koynov, W. Knoll, Q. Li, *Angew. Chem. Int. Ed.* **2009**, *48*, 4598.

[19] B. Mohammed, F. V. D. Kammer, M. Motelica-Heino, P. l. Coustumer, *Anal. Bioanal. Chem.* **2005**, *383*, 549.

[20] a) J. P. Hill, W. S. Jin, A. Kosaka, T. Fukushima, H. Ichihara, T. Shimomura, K. Ito, T. Hashizume, N. Ishii, T. Aida, *Science* **2004**, *304*, 1481; b) J. Duering, A. Hoelzer, U. Kolb, R. Branscheid, F. Groehn, *Angew. Chem. Int. Ed.* **2013**, *52*, 8742.

[21] R. Zana, *Surfactant Solutions: New Methods of Investigation*, Marcel Dekker, New York **1986**.

[22] S. Mann, *Nat. Mater.* **2009**, *8*, 781.

[23] Y. Dong, R. Wang, G. Li, C. Chen, Y. Chi, G. Chen, *Anal. Chem.* **2012**, *84*, 6220.

[24] L. Zhou, Y. Lin, Z. Huang, J. Ren, X. Qu, *Chem. Commun.* **2012**, *48*, 1147.

[25] S. Koga, D. S. Williams, A. W. Perriman, S. Mann, *Nat. Chem.* **2011**, *3*, 720.

[26] C. Liu, P. Zhang, F. Tian, W. Li, F. Li, W. Liu, *J. Mater. Chem.* **2011**, *21*, 13163.

[27] a) Y. P. Myer, *Macromolecules* **1969**, *2*, 624; b) S. Watanabe, T. Saito, *Int. J. Pept. Protein Res.* **1985**, *26*, 439.

[28] a) S. G. Elci, D. F. Moyano, S. Rana, G. Y. Tong, R. L. Phillips, U. H. F. Bunz, V. M. Rotello, *Chem. Sci.* **2013**, *4*, 2076; b) S. M. Bromfield, A. Barnard, P. Posocco, M. Fermeglia, S. Pricl, D. K. Smith, *J. Am. Chem. Soc.* **2013**, *135*, 2911.

[29] A. Shvarev, E. Bakker, *J. Am. Chem. Soc.* **2003**, *125*, 11192.

[30] L. B. Jaques, *Pharmacol. Rev.* **1979**, *31*, 99.

[31] P. D. T. Huibers, *Langmuir* **1999**, *15*, 7546.

[32] M. De, S. Rana, H. Akpinar, O. R. Miranda, R. R. Arvizo, U. H. F. Bunz, V. M. Rotello, *Nat. Chem.* **2009**, *1*, 461.

[33] J. Han, K. Burgess, *Chem. Rev.* **2010**, *110*, 2709.

[34] a) H. Wu, L. Zhu, V. P. Torchilin, *Biomaterials* **2013**, *34*, 1213; b) R. Liu, D. Li, B. He, X. Xu, M. Sheng, Y. Lai, G. Wang, Z. Gu, *J. Controlled Release* **2011**, *152*, 49.

[35] S. Girod, M. Boissere, K. Longchambon, S. Begu, C. Tourne-Petheil, J. M. Devoisselle, *Carbohydr. Polym.* **2004**, *55*, 37.

[36] L. Roxvall, A. Bengtson, L. Sennerby, M. Heideman, *Biol. Chem. Hoppe-Seyler* **1991**, *372*, 273.

[37] a) M. F. Byrne, R. M. Mitchell, H. Stiffler, P. S. Jowell, M. S. Branch, T. N. Pappas, D. Tyler, J. Baillie, *Can. J. Gastroenterol.* **2002**, *16*, 849; b) M. Hirota, M. Ohmuraya, H. Baba, *J. Gastroenterol.* **2006**, *41*, 832.

[38] Y. Lin, R. Chapman, M. M. Stevens, *Anal. Chem.* **2014**, *86*, 6410.

[39] a) J. E. Ghadiali, M. M. Stevens, *Adv. Mater.* **2008**, *20*, 4359; b) S. B. Lowe, J. A. G. Dick, B. E. Cohen, M. M. Stevens, *ACS Nano* **2012**, *6*, 851.

[40] H. Tao, K. Yang, Z. Ma, J. Wan, Y. Zhang, Z. Kang, Z. Liu, *Small* **2012**, *8*, 281.

[41] K. Devanand, J. C. Selser, *Macromolecules* **1991**, *24*, 5943.